catalysts

MDPI

Article

Fe_3O_4-Zeolite Hybrid Material as Hetero-Fenton Catalyst for Enhanced Degradation of Aqueous Ofloxacin Solution

Alamri Rahmah Dhahawi Ahmad, Saifullahi Shehu Imam, Wen Da Oh and Rohana Adnan *

School of Chemical Sciences, Universiti Sains Malaysia, Penang 11800, Malaysia; ralamri-1406@outlook.com (A.R.D.A.); ssimam.chm@buk.edu.ng (S.S.I.); ohwenda@usm.my (W.D.O.)

* Correspondence: r_adnan@usm.my

Received: 11 September 2020; Accepted: 22 October 2020; Published: 27 October 2020

Abstract: A hetero-Fenton catalyst comprising of Fe_3O_4 nanoparticles loaded on zeolite (FeZ) has been synthesized using a facile co-precipitation method. The catalyst was characterized using various characterization methods and then, subsequently, was used to degrade ofloxacin (OFL, 20 mg·L^{-1}), an antibiotic, via a heterogeneous Fenton process in the presence of an oxidizing agent. The effects of different parameters such as Fe_3O_4 loading on zeolite, catalyst loading, initial solution pH, initial OFL concentration, different oxidants, H_2O_2 dosage, reaction temperature, and inorganic salts were studied to determine the performance of the FeZ catalyst towards Fenton degradation of OFL under different conditions. Experimental results revealed that as much as 88% OFL and 51.2% total organic carbon (TOC) could be removed in 120 min using the FeZ catalyst. Moreover, the FeZ composite catalyst showed good stability for Fenton degradation of OFL even after five cycles, indicating that the FeZ catalyst could be a good candidate for wastewater remediation.

Keywords: Fenton degradation; ofloxacin; Fe_3O_4; zeolite; heterogeneous

1. Introduction

Ofloxacin (OFL) (Figure 1) is a second-generation fluoroquinolone antibiotic with the chemical formula $C_{18}H_{20}FN_3O_4$ and the chemical name 9-fluoro-2,3-dihydro-3-methyl-10-(4-methyl-1-piperazynyl)-7-oxo-7H-pyrido-[1,2,3-de]-1,4-benzoxazine-6-carboxylic acid [1,2]. It was patented in 1980 and subsequently approved for medical use in 1985 [3,4]. Currently, OFL is frequently prescribed for the treatment of various bacterial infections that cause digestive, respiratory, gastrointestinal, and urinary tract infections [5,6]. However, due to its partial metabolism in the body after ingestion, biological resistance, and the large volume of pharmaceutical wastewater which has been released untreated, studies have reported the detection of OFL with different concentrations in hospital wastewater (25,000–35,000 ng·L^{-1}), municipal wastewater treatment plants (53–1800 ng·L^{-1}), and surface water (10–535 ng·L^{-1}), with a residence time of about 10.6 days [7–9]. The presence of OFL in water results in unpleasant odors [10]. Besides, it may also lead to microbial resistance among pathogens or the death of microorganisms that are effective in wastewater remediation [7,10]. Although, currently, pharmaceutical compounds, including OFL, belong to the emerging pollutants category that is still not regulated by water quality laws, the identification of proper process(es) for their complete elimination from wastewater is imperative [11].

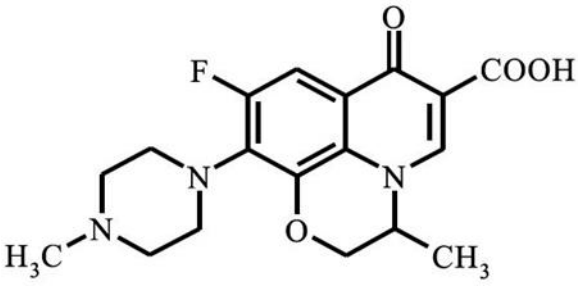

Figure 1. Chemical structure of ofloxacin (OFL).

Unfortunately, the techniques employed by most wastewater treatment plants (WWTPs) have limited capacity for the thorough elimination of pharmaceuticals and personal care products (PPCPs) from wastewater, as they are not originally designed for removing PPCPs [12]. Furthermore, certain physical and biological methods that are also being employed have some limitations. For instance, most of the physical treatment methods only transfer the pollutants to another phase rather than destroying them [12]. Likewise, a biological treatment method, such as biodegradation, could lead to the development of antibiotic-resistant bacteria [13].

Unlike the physical and biological treatment methods, chemical oxidation methods such as homogeneous and heterogeneous Fenton treatment methods are capable of mineralizing a wide range of organic pollutants [14]. However, compared to the homogeneous Fenton process, the easy recovery of the catalyst after application in the case of a heterogeneous Fenton process makes it more convenient [15]. Following that, many researchers have reported various methods of enhancing the efficiency of a heterogeneous Fenton process. The common method involves immobilizing the metallic ions/oxides onto various supports. Such supports, including activated carbon [16], carbon nanotubes [17], graphite oxide [18], SBA-15 [19], etc., are capable of improving the efficiency of the Fenton process, and also ease the catalyst recovery process after application. In the current work, Fe_3O_4-zeolite composites will be synthesized via a co-precipitation method for subsequent use as a catalyst in a heterogeneous Fenton process. To the best of our knowledge, there have been no studies on the heterogeneous Fenton degradation of OFL using zeolite-supported magnetite (Fe_3O_4-zeolite). This work reports the facile production of Fe_3O_4-zeolite as a low-cost catalyst for the heterogeneous Fenton degradation using a widely available and abundant material. In addition, zeolite has been used previously for the adsorption of organic pollutants [20,21]. The ability of zeolite to behave as an adsorbent implies a greater possibility of contact between catalyst and pollutant. Such a process will improve the efficiency of the Fenton reaction.

2. Results and Discussion

2.1. X-ray Photoelectron Spectroscopy (XPS) Analysis

The elemental composition and the interaction between Fe_3O_4 and zeolite in FeZ composites were studied using XPS analysis in the region of 0–1200 eV, and the results are shown in Figure 2. Based on the survey spectra presented in Figure 2a, C, O, Na, Al, and Si are present on the surface of bare zeolite, while the survey spectra in Figure 2b–f confirmed the coexistence of C, O, Al, Si, and Fe in the FeZ composites.

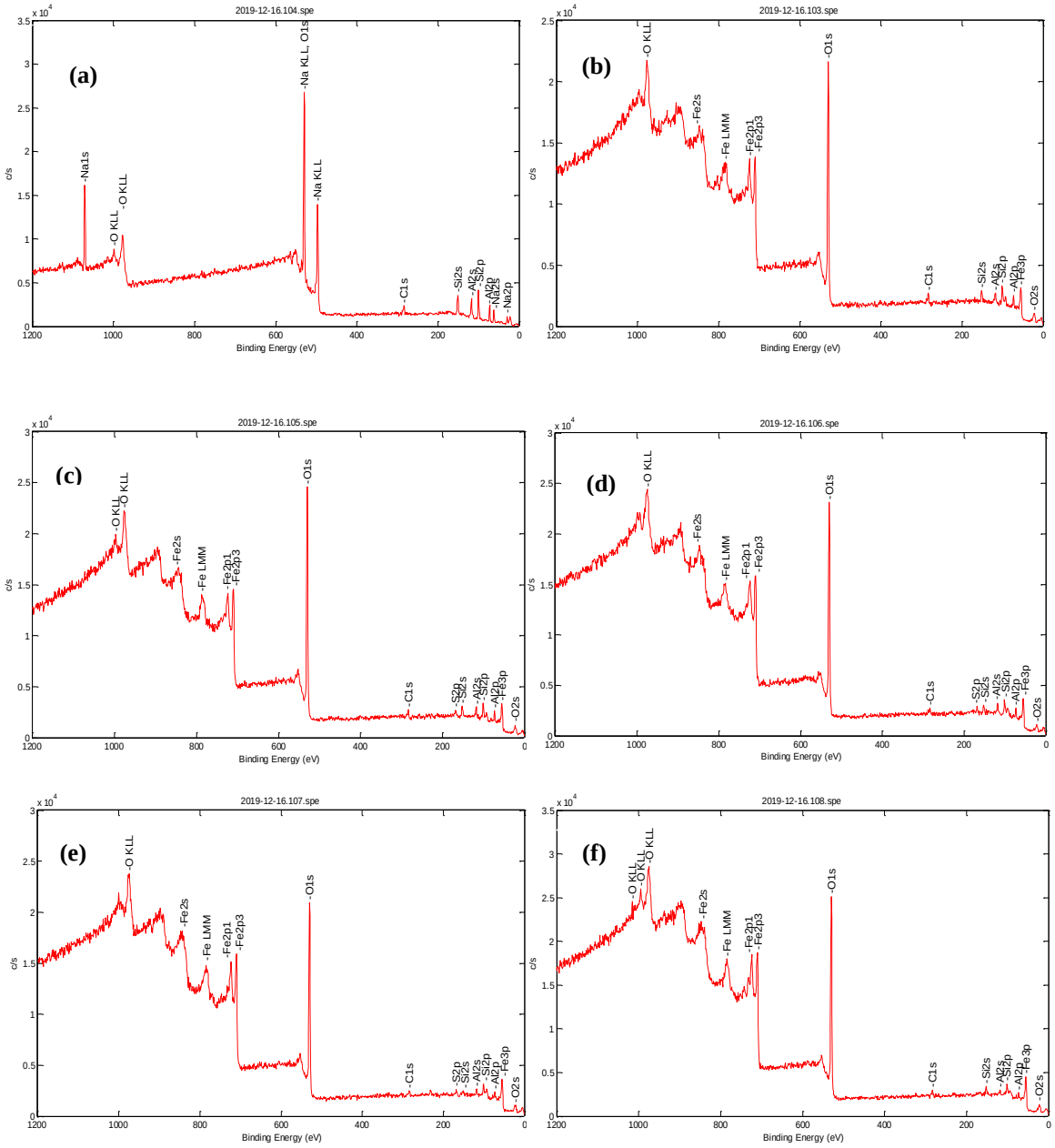

Figure 2. XPS spectra of (**a**) bare zeolite, (**b**) FeZ-1.5, (**c**) FeZ-3, (**d**) FeZ-5, (**e**) FeZ-8, and (**f**) FeZ-10 composites.

Within the FeZ composites spectra, two peaks with the binding energy of 710 and 725 eV are attributed to Fe $2p_{3/2}$ and Fe $2p_{1/2}$, indicating the presence of Fe_3O_4 [22]. Meanwhile, the peak around 95 eV also indicates the existence of Fe_3O_4 [23]. These results have proved the existence of iron oxide in the form of Fe_3O_4 in FeZ composites. The O 1s peak at 530 eV belongs to O^{2-} [24]. The presence of a peak centered at 286 eV is attributed to the presence of elemental carbon (C 1s) from the carbon band used during sample preparation. No other impurities were detected.

Finally, the XPS analysis result revealed that there is no Na^+ ion in the survey spectra of the FeZ composites. Such an effect is attributed to the exchange of sodium ions with iron ions in the interlayer of zeolite [25]. Based on the XPS analysis results, it is believed that composites of zeolite loaded with variable amounts of Fe_3O_4 have been successfully synthesized.

2.2. Fourier Transform Infrared (FTIR) Analysis

The functional groups present in bare zeolite and in FeZ composites were also studied using FTIR spectrometer, and the results are shown in Figure 3. In the case of bare zeolite, the absorption bands at 1020 and 440 cm^{-1} are due to Si–O–Si stretching and bending vibrations, respectively. Meanwhile, the absorption band at 532 cm^{-1} is due to Al–O–Si deformation [26]. However, the intensities of the peaks at 440 and 532 cm^{-1} attributed to Si–O–Si and Al–O–Si decrease significantly due to the loading of zeolite with Fe_3O_4. The peaks at 3500 and 1650 cm^{-1} are due to the stretching and bending vibrations of hydroxyl groups of absorbed water molecules, respectively [25]. In the case of FeZ composites, the band at 583 cm^{-1} is attributed to the stretching vibration of Fe–O [27], which confirmed the existence of Fe_3O_4 in FeZ composites [28]. The absence of such band in FeZ-1.5 and FeZ-3 composites might be attributed to the low amount of magnetite in the composites. Furthermore, the small peak at around 1450 cm^{-1} in the FeZ composites is due to the remnant of NH_3 used during composites preparation [25].

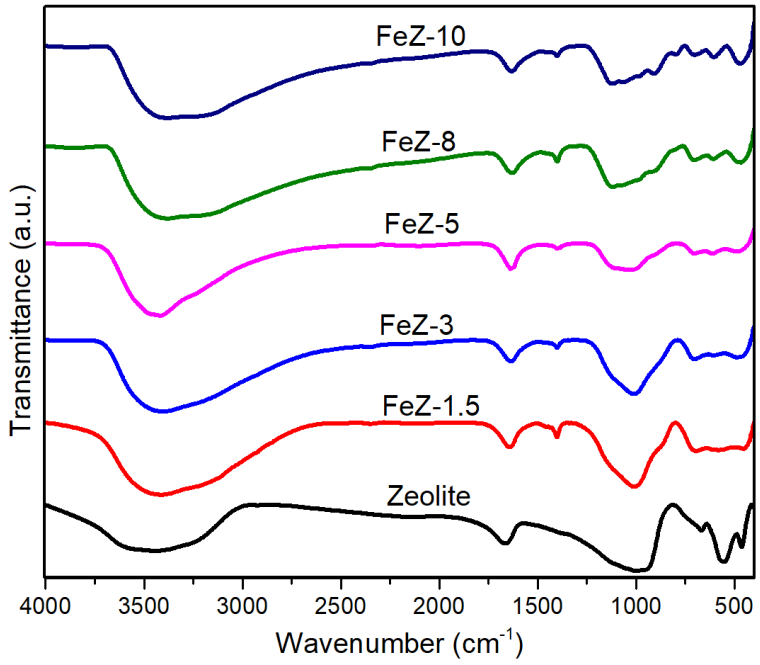

Figure 3. FTIR spectra of bare zeolite and FeZ composites.

2.3. Field Emission Scanning Electron Microscopy (FESEM)/Energy Dispersive X-ray (EDX) Analysis

FESEM images of bare zeolite and FeZ composites are shown in Figure 4. Based on the image presented in Figure 4a, bare zeolite is made up of various sized particles with an irregular shape, and the surface is virtually smooth. However, in the case of FeZ composites in Figure 4b–f, the surface is rough, and this could be due to the presence of Fe_3O_4 particles in the form of clusters or nanoparticles on the surface of the zeolite. Among the FeZ composites, the zeolite matrix is still clearly observable in the case of FeZ-1.5, FeZ-3, and FeZ-5 composites, which contain a low amount of Fe_3O_4 loading during synthesis. However, at a higher amount of Fe_3O_4, such as FeZ-8 and FeZ-10 composites, the presence of zeolite matrix cannot be detected.

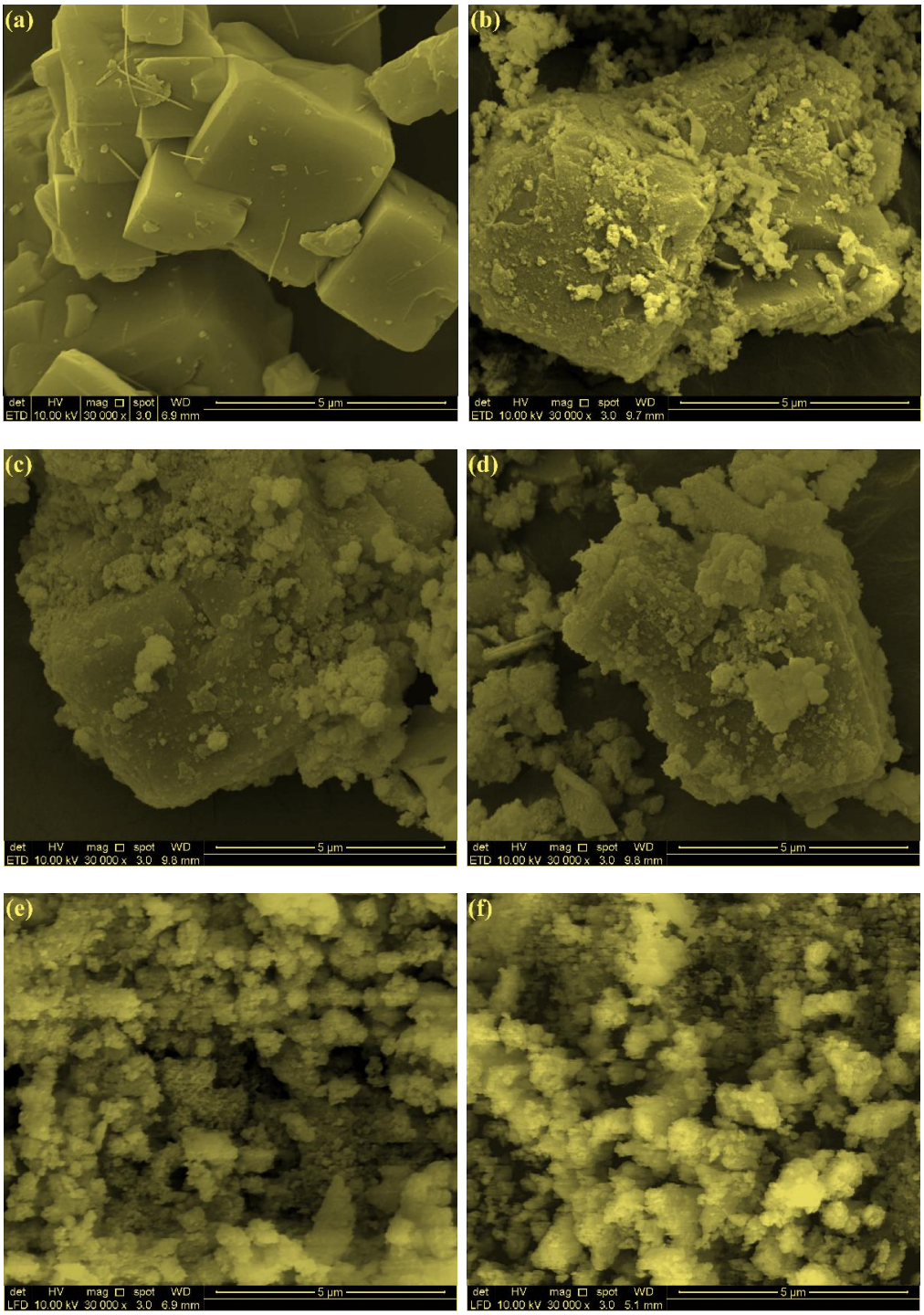

Figure 4. FESEM images of zeolite (**a**), FeZ-1.5 (**b**), FeZ-3 (**c**), FeZ-5 (**d**), FeZ-8 (**e**), and FeZ-10 (**f**) composites.

Furthermore, the elemental composition of bare zeolite and FeZ composites obtained from EDS analysis is shown in Table 1. The results revealed the presence of Na, Al, O, and Si in bare zeolite and Fe, Al, O, and Si in FeZ composites. The absence of Na in FeZ composites could be explained due to the ion exchange reaction with Fe ions. Moreover, the concentration of Fe in the FeZ composites keeps on increasing with the increase in the amount of loaded magnetite. Such results are a further indication that Fe_3O_4 has been immobilized onto zeolite.

Table 1. Composition of bare zeolite and FeZ composites as determined by EDX.

Sample	Al%	Si%	Na%	O%	Fe%
Zeolite	16.76	18.69	14.40	50.15	-
FeZ-1.5	17.81	17.84	-	41.67	22.68
FeZ-3	15.20	15.77	-	40.00	29.03
FeZ-5	15.02	13.91	-	39.47	31.59
FeZ-8	4.12	4.39	-	38.88	52.62
FeZ-10	4.09	4.01	-	35.60	56.29

2.4. Transmission Electron Microscopy (TEM) Analysis

The morphology of pristine zeolite and FeZ composites was further studied using TEM, and the results are shown in Figure 5. Based on the image presented in Figure 5a, pristine zeolite is composed of irregularly shaped particles with a smooth surface. In the case of FeZ composites shown in Figure 5b–f, some new particles apart from that of pristine zeolite were observed in the composites. The amount of the particles increases with the increase in the amount of Fe_3O_4 nanoparticles being immobilized onto zeolite. The change in morphology to hair-like particles was observed at higher magnetite concentration. In general, despite subjecting the FeZ composites to strong ultrasonication treatment during TEM sample preparation, the Fe_3O_4 nanoparticles could still be found on the zeolite surface. This indicates a strong interaction between Fe_3O_4 nanoparticles and zeolite.

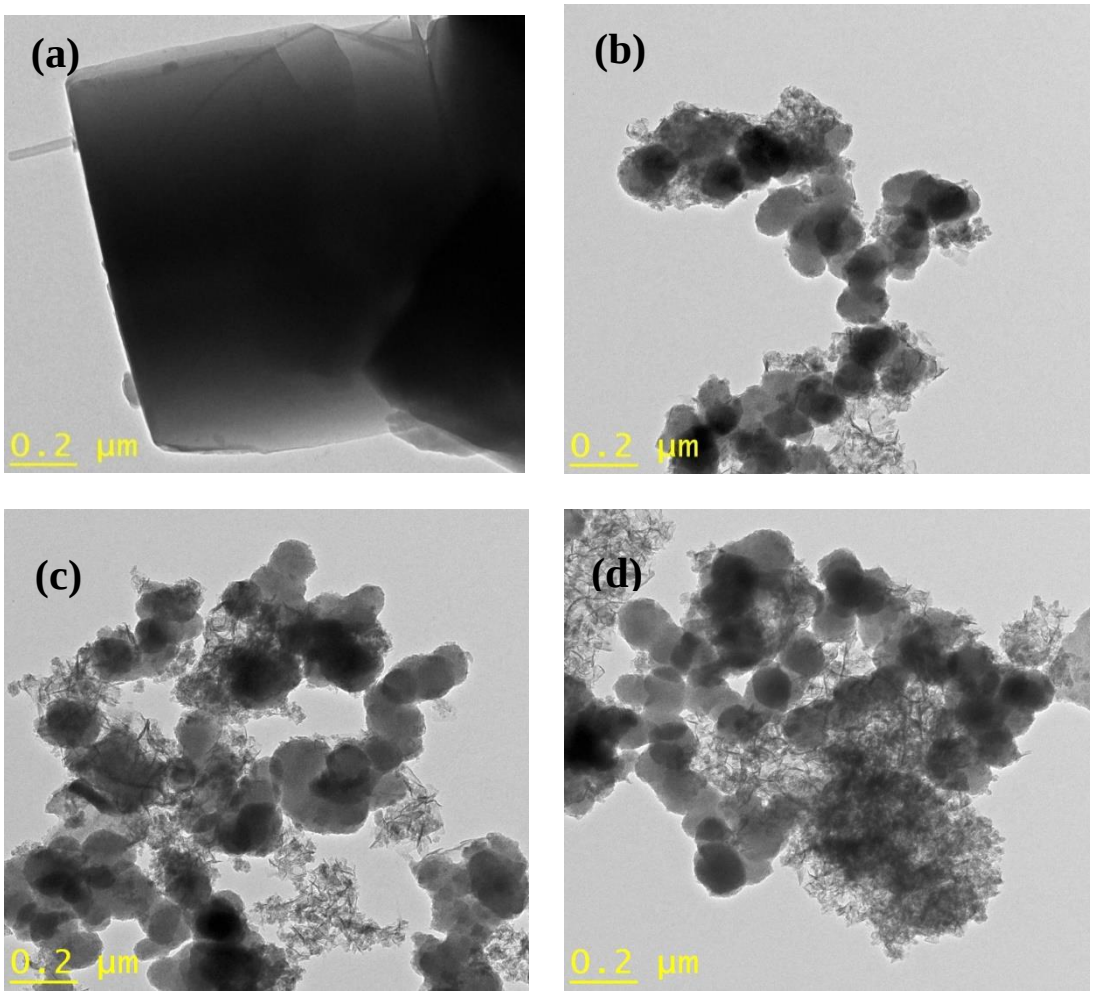

Figure 5. *Cont.*

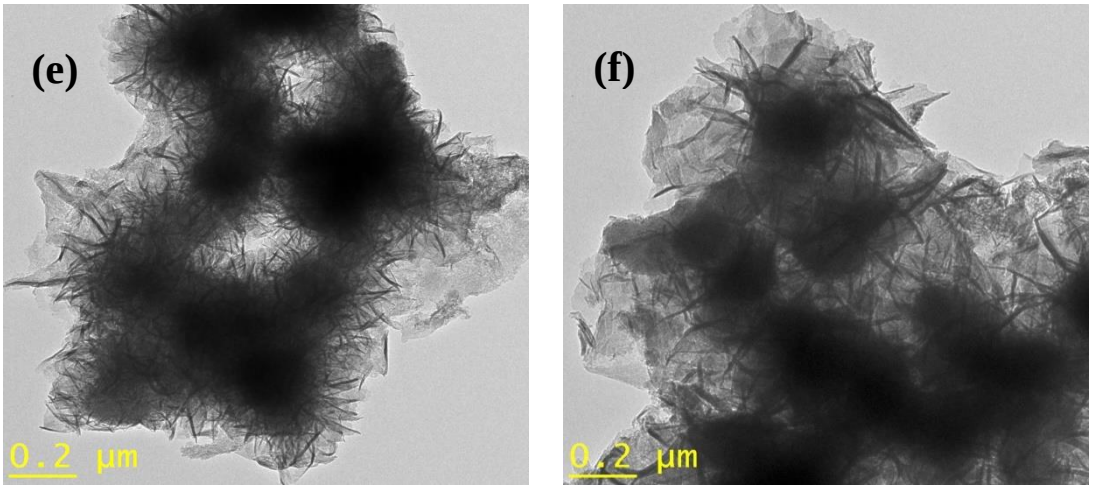

Figure 5. TEM images of zeolite (**a**), FeZ-1.5 (**b**), FeZ-3 (**c**), FeZ-5 (**d**), FeZ-8 (**e**), and FeZ-10 (**f**) composites.

2.5. Nitrogen Adsorption-Desorption Analysis

Nitrogen adsorption–desorption isotherms and Barrett-Joyner-Halender (BJH) pore size distribution (insets) of bare zeolite and FeZ composites are shown in Figure S1, and their structural details are summarized in Table 2. Although both bare zeolite and FeZ composites have type IV isotherms, FeZ composites have a distinct hysteresis loop in the range of P/P_0 0.4–1.0, due to capillary condensation of mesopores between closely packed spherical particles [29]. However, the adsorption capacities of the FeZ composites for N_2 are higher than that of bare zeolite and increase by as much as 160-fold as compared to zeolite alone. In addition, the shapes of the adsorption-desorption isotherms and pore size distributions of FeZ composites are different from that of bare zeolite, indicating the change in the pore structure due to the presence of Fe_3O_4 [30]. Furthermore, from the data presented in Table 2, the bare zeolite used has a low surface area (1.52 $m^2 \cdot g^{-1}$). However, the surface area of FeZ composites increased up to 251.6 $m^2 \cdot g^{-1}$ and decreases slightly to 211 $m^2 \cdot g^{-1}$ for FeZ-10. The decrease could be attributed to the agglomeration of Fe_3O_4 particles at higher loading. From the pore size distribution curves (insets), zeolite is polymodal. However, loading of Fe_3O_4 onto zeolite leads to the decrease in the pore size, an effect attributed to the blocking of zeolite pores by the magnetite. Meanwhile, the pore size distribution curve of FeZ-10 is bimodal, and this can be explained due to the formation of pores between the excess magnetite.

Table 2. Surface area and pore volume of bare zeolite and FeZ composites.

Samples	BET Surface Area ($m^2 \cdot g^{-1}$)	Pore Volume ($cm^3 \cdot g^{-1}$)
Zeolite	1.52	0.001798
FeZ-1.5	70.91	0.202736
FeZ-3	251.60	0.317371
FeZ-5	251.53	0.276022
FeZ-8	220.52	0.273748
FeZ-10	211.96	0.262692

2.6. Fenton Oxidation Activity of FeZ Composites

2.6.1. OFL Removal in Different Processes

Initially, a series of control experiments were conducted to determine the performance of (i) raw zeolite + OFL, (ii) H_2O_2 + OFL, (iii) Fe_3O_4-zeolite + OFL, (iv) zeolite + H_2O_2, and (v) Fe_3O_4-zeolite + H_2O_2 + OFL towards the removal of OFL. The Fe_3O_4-zeolite composite used for this study is FeZ-8, and the results are shown in Figure 6.

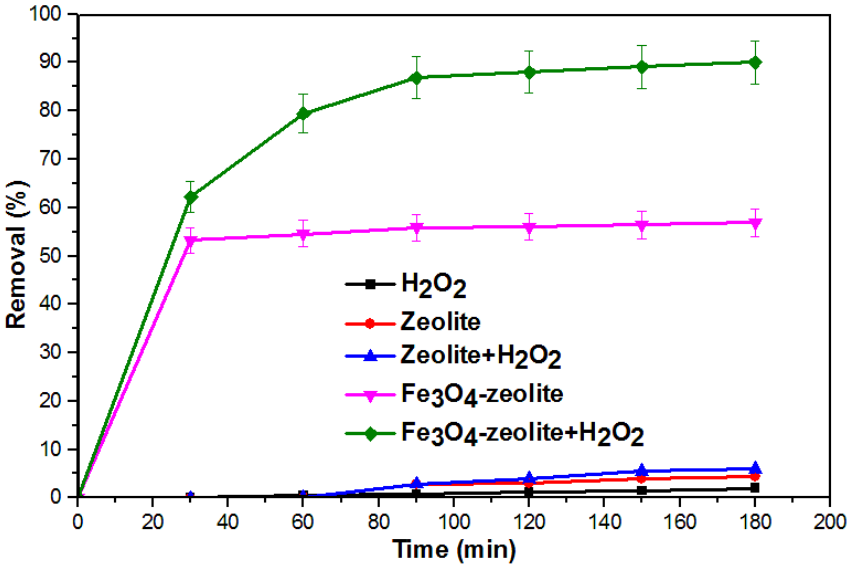

Figure 6. Removal efficiencies of OFL in different processes.

As shown in Figure 6, only 2% degradation was achieved after 180 min in the presence of H_2O_2 alone, which indicates that degradation under H_2O_2 is minimal. The results of such nature could be due to the low oxidation potential of H_2O_2 as compared to its $HO^{\bullet}$ [31]. In the case of bare zeolite, the low percentage of removal of OFL (4%) achieved is attributed to its adsorption capability. The addition of H_2O_2 onto bare zeolite did not improve the efficiency, since zeolite is not capable of dissociating H_2O_2 to produce $HO^{\bullet}$. Previously, Hu, et al. [32] also reported similar results. Meanwhile, Fe_3O_4-zeolite was able to adsorb up to 56.9% of OFL from the aqueous solution. This indicates that loading Fe_3O_4 onto bare zeolite leads to the formation of composites with higher adsorption capability towards OFL. On the other hand, in the presence of H_2O_2, the performance of Fe_3O_4-zeolite increased significantly to about 90%, thus indicating the reaction occurs via Fenton oxidation. Such results imply that Fe_3O_4-zeolite exhibited an excellent catalytic ability to activate H_2O_2, which is useful for Fenton reaction [33]. The results also confirmed the synergetic effect between Fe_3O_4-zeolite and H_2O_2 is necessary to achieve higher efficiency, and that dissociation of H_2O_2 is mainly caused by Fe_3O_4. The results obtained for the Fenton degradation of OFL using Fe_3O_4-zeolite composite was compared with the previous results reported for the Fenton degradation of OFL using different catalysts, and the results are shown in Table 3. The performance recorded using the Fe_3O_4-zeolite composite is encouraging and therefore, suggests that FeZ is a potential candidate for the treatment of wastewater contaminated by OFL.

Table 3. Comparison of Fenton catalytic performance in the removal of OFL.

Samples	Conc. of OFL ($mg \cdot L^{-1}$)	Catalyst Dosage ($g \cdot L^{-1}$)	Time (min)	pH	H_2O_2 Conc.	% Removal	Ref.
D-FeCu@Sep	10	3.0	120	5.0	0.03 M	~100	[34]
A-FeCu@Sep	10	3.0	120	5.0	0.03 M	~40	[34]
S-doped ZnO	10	0.25	120	6.5	5 $mL \cdot L^{-1}$	23	[35]
Fe_3O_4	10	0.25	120	6.5	5 $mL \cdot L^{-1}$	~60	[35]
Fe_3O_4@S-doped ZnO	10	0.25	120	6.5	5 $mL \cdot L^{-1}$	~100	[35]
AC-Fe_3O_4	12	0.5	60	3.3	20.0 mM	~75	[36]
Fe_3O_4-CeO_2	12	0.5	60	3.3	20.0 mM	~80	[36]
Fe_3O_4-CeO_2/AC	12	0.5	60	3.3	20.0 mM	~98	[36]
Fe@Mpsi	30	1.0	120	Initial pH	2000 $mg \cdot L^{-1}$	18	[37]
Cu@Mpsi	30	1.0	120	Initial pH	2000 $mg \cdot L^{-1}$	51	[37]
Fe-Cu@SBA-15	30	1.0	120	Initial pH	2000 $mg \cdot L^{-1}$	~70	[37]
Fe-Cu@Mpsi	30	1.0	120	Initial pH	2000 $mg \cdot L^{-1}$	~82	[37]
Fe_3O_4-zeolite	20	1.0	120	9	5 $mL \cdot L^{-1}$	88	Present work

2.6.2. Effect of Fe_3O_4 Loading on Zeolite

The amount of Fe_3O_4 loading on zeolite is expected to play a vital role in the overall Fenton oxidation process, since it controls the iron ions concentration and the HO• production rate [38]. For these purposes, the effect of Fe_3O_4 loading on zeolite was studied by varying the amount of Fe_3O_4 from 1.5 to 10 mmol, and the results are shown in Figure 7a. Subsequently, the experimental data were examined using the zero-order, pseudo-first-order, and pseudo-second-order kinetic models and the results are shown in Figure S2. Based on the kinetic data presented in Table S1 and the values of the correlation coefficient, R^2, the Fenton degradation of OFL using FeZ composites follows the pseudo-first-order kinetic model.

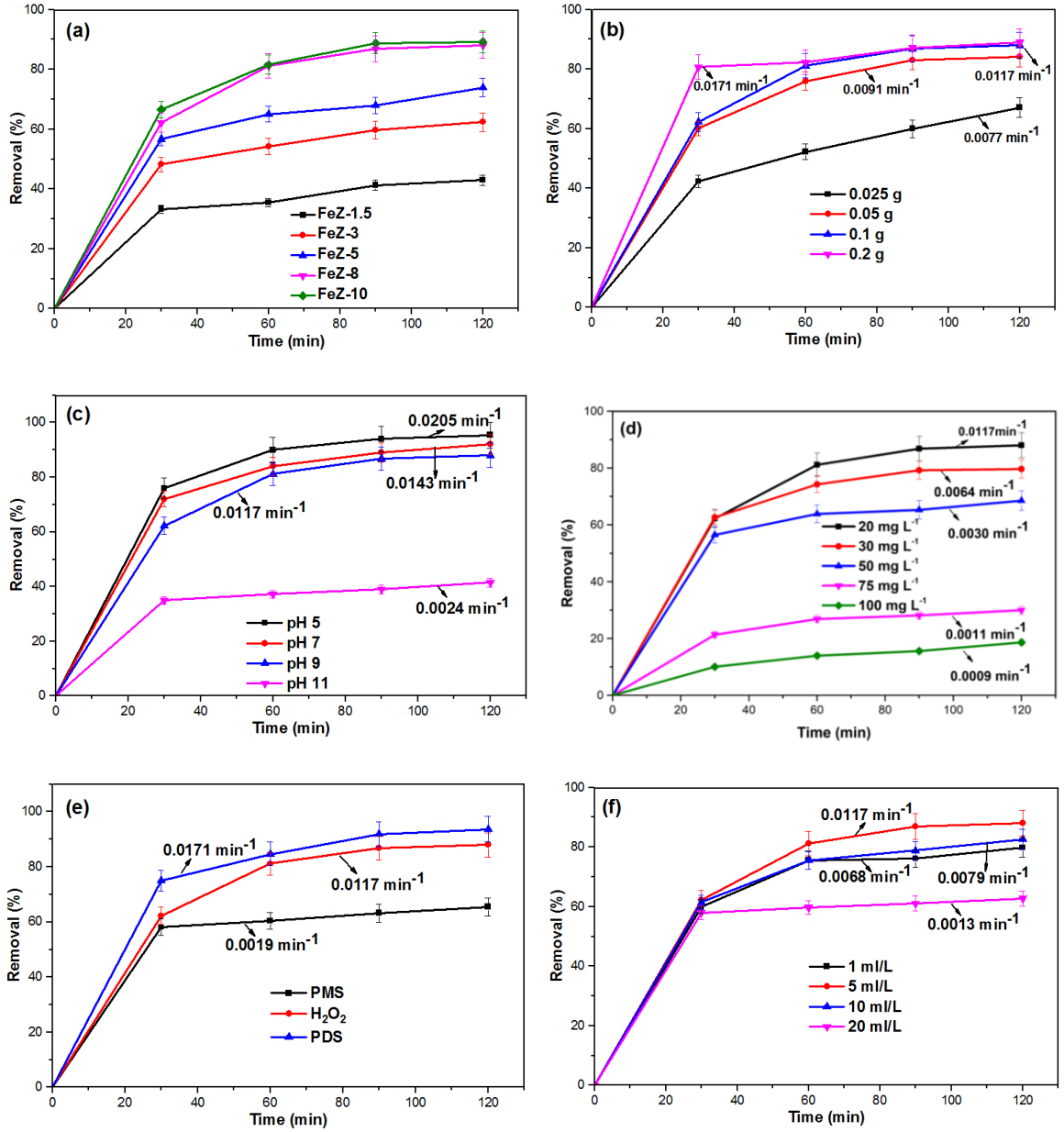

Figure 7. *Cont.*

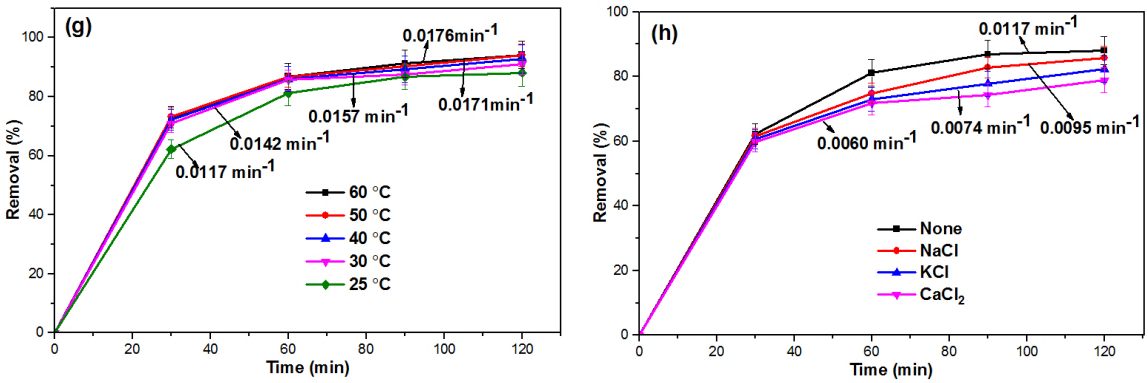

Figure 7. Effects of (**a**) Fe_3O_4 loading on zeolite, (**b**) FeZ-8 catalyst dosage, (**c**) initial solution pH, (**d**) initial OFL concentration, (**e**) different oxidants, (**f**) H_2O_2 dosage, (**g**) reaction temperature, and (**h**) inorganic ions on the Fenton degradation of OFL. Unless stated otherwise, reaction conditions are based on: [OFL] = 20 mg·L^{-1}, pH = 9, (FeZ-8) = 1 g·L^{-1}, (H_2O_2) = 5 mL·L^{-1}.

Furthermore, as the amount of Fe_3O_4 in the FeZ composite increases from 1.5 to 8 mmol, the degradation rate also increases. Such an effect is attributed to the increase in the production of HO• by higher amount of iron ions. This, however, is contrary to the earlier surface area results presented in Table 2, where FeZ-3 and FeZ-5 (with low loading of Fe_3O_4) have higher surface areas than FeZ-8 and FeZ-10. This could be explained by the fact that FeZ-8 and FeZ-10 have a higher concentration of iron ions. However, the degradation rate by FeZ-10 is virtually similar to the performance recorded using FeZ-8. Previously, Hassan and Hameed [31] have also reported that at a higher concentration, the excess Fe_3O_4 would instead scavenge •OH. Therefore, for the rest of the study, FeZ-8 was used to investigate the effect of experimental parameters on the degradation of OFL by the FeZ composite. In general, the results from this study have further confirmed the indispensable role of the Fe_3O_4-zeolite composite catalyst in the Fenton degradation process.

2.6.3. Effect of Catalyst Dosage

The effect of FeZ-8 catalyst dosage was studied using 0.025, 0.05, 0.1, and 0.2 g catalyst loading, and the results are shown in Figure 7b. As the catalyst dosage increases, the degradation efficiency and the rate also increase. Such effect is due to the increased contact of OFL and H_2O_2 with the high amount of FeZ-8 catalyst [39]. Previously, Shukla, et al. [40] have attributed such performance to the dual effect of combined adsorption and oxidation. However, the increase in degradation efficiency in the same reaction time, when the catalyst dosage was increased from 0.1 to 0.2 g is not appreciable. According to Nguyen, et al. [41], this could be due the fact that at high iron content, the catalyst behaves as an HO• scavenger, and therefore, no significant increase in degradation efficiency could be observed.

2.6.4. Effect of Initial Solution pH

Apart from the performance recorded at the initial solution pH (pH 9.0), the effect of initial solution pH on the Fenton degradation of OFL in FeZ-8 + H_2O_2 system was determined at pH range of 5–11 and the results are shown in Figure 7c. It is obvious that the percentage of OFL removal efficiency and degradation rate keeps on decreasing with the increase in pH from 5 to 11. This could be explained using the favorable interaction at lower pH values compared to the interaction between the OFL molecules and the FeZ-8 catalyst at higher pH values, since the FeZ-8 catalyst has the pH at point of zero charge (pH_{zpc}) of 4.3, and the OFL has the acid dissociation constants values, pKa_1 = 5.98 and pKa_2 = 8.00 [42]. Furthermore, the enhanced generation of HO• at lower pH values could be another contributing factor to the high performance recorded [43]. Meanwhile, the formation of oxyhydroxides like $Fe(OH)_3$ and $FeOH^+$ at higher pH values, which have been adsorbed onto the surface of the FeZ-8 catalyst, contributes to the decrease in degradation efficiency with the increase in pH [44]. Yet still, the

performance recorded in pH 5–9 is appreciable. The significant decrease in performance at pH 11 is attributed to the decrease in the oxidation potential of $HO^{\bullet}$ and the formation of inactive ferryl ions (FeO^{2+}) at higher pH [45]. However, the result obtained is a tremendous achievement since it shows that the FeZ-8 catalyst could function well within a wide pH range. This is important because the pH range of wastewater is between 5.5 and 9.0 [46].

2.6.5. Effect of Initial OFL Concentration

The effect of initial OFL concentration on the performance of FeZ-8 was studied using OFL solutions with a concentration between 20 and 100 mg·L^{-1}, while other parameters are kept constant, and the results are shown in Figure 7d. The heterogeneous Fenton degradation of OFL using the FeZ-8 catalyst occurs at the surface of the catalyst. It involves the reaction between the generated $HO^{\bullet}$ at the active sites, together with the adsorbed OFL molecules [31]. In this study, since the dose of FeZ-8 and the concentration of H_2O_2 are constant, the number of hydroxyl radicals produced in the systems is also the same. Thus, the decrease in the degradation efficiency with the increase in OFL concentration is attributed to the low amount of hydroxyl radicals in the system compared to the available OFL molecules.

2.6.6. Effect of Different Oxidants

The effect of different oxidants—peroxydisulfate (PDS), hydrogen peroxide (H_2O_2), and peroxomonosulfate (PMS)—on the catalytic degradation of OFL was also studied. This study was conducted by activating PDS, PMS, and H_2O_2 with FeZ-8 to produce $SO_4^{\bullet-}$ and $HO^{\bullet}$. Based on the results shown in Figure 7e, the order of reactivity is PDS > H_2O_2 > PMS. The reaction of Fe^{2+} with PS, H_2O_2, and PMS could be presented in Equations (1)–(3) [47].

$$Fe^{2+} + H_2O_2 \rightarrow Fe^{3+} + OH^- + HO^{\bullet} \quad (1)$$

$$Fe^{2+} + S_2O_8^{2-} \rightarrow Fe^{3+} + SO_4^{\bullet-} + SO_4^{2-} \quad (2)$$

$$Fe^{2+} + HSO_5^- \rightarrow Fe^{3+} + SO_4^{\bullet-} + OH^- \quad (3)$$

In the case of PDS and H_2O_2, the high performance in FeZ-8/PDS than FeZ-8/H_2O_2 is due to the rapid formation of reactive oxygen species (ROSs) from PDS activation [48]. In the case of PMS, the inherent pH of aqueous OFL solution is 9. The low performance recorded at this pH could be attributed to the self-dissociation of PMS, which is reported to occur at high pH through non-radical pathways [49].

2.6.7. Effect of H_2O_2 Dosage

The effect of H_2O_2 dosage on the Fenton degradation of OFL was studied by varying the amount of H_2O_2 from 1 to 20 mL·L^{-1} and the results are shown in Figure 7f. From the results obtained, an increase in H_2O_2 concentration from 1 to 5 mL·L^{-1} resulted in an increase in the Fenton degradation rate from 0.0068 to 0.0118 min^{-1}. Such an effect is attributed to the rise in the number of $HO^{\bullet}$. However, a further increase in H_2O_2 concentration from 5 to 20 mL·L^{-1} causes a decrease in Fenton degradation rate to 0.0013 min^{-1}. This could be explained because of the excess H_2O_2 acting as a hydroxyl radical scavenger to form the less reactive hydroperoxyl radicals ($HOO^{\bullet}$), which do not contribute much to the oxidation reaction [50].

2.6.8. Effect of Reaction Temperature

The effect of reaction temperature on the Fenton degradation of OFL using the FeZ-8 catalyst has been studied, and the results are depicted in Figure 7g. From the figure, a higher reaction temperature resulted in a little bit higher degradation of OFL, which is in agreement with the report by Soon and Hameed [39]. The authors stated that higher temperature accelerates the decomposition of H_2O_2

into HO•. In general, the findings show that the Fenton degradation of OFL by the FeZ-8 catalyst was not very sensitive to the reaction temperature. Furthermore, the activation energy (E_a) for the Fenton degradation of OFL using the FeZ-8 catalyst was estimated using the plot of ln k against 1/T, based on the Arrhenius equation $\ln k = \ln A - E_a/RT$, where k is the rate constant, R is the universal gas constant (8.314 J mol^{-1} K^{-1}), and A is pre-exponential factor, and the results are shown in Figure S3. Using the slope of the plot, the E_a value was obtained as 8.8860 kJ mol^{-1} and thus, indicates low reaction activation energy [51]. Such a value, which is significantly lower than the 213.8 kJ mol^{-1} for the dissociation of H_2O_2 to HO• [52], confirms the catalytic property of FeZ-8.

2.6.9. Effect of Inorganic Salts

Apart from organic pollutants, real wastewater often contains some inorganic salts, which could possibly affect the efficiency of the degradation process during the Fenton reaction. For this purpose, 10 mmol of NaCl, KCl, and $CaCl_2$ salts were separately introduced during the Fenton degradation of OFL, and the results are shown in Figure 7h. Although no significant decrease in degradation efficiency of OFL was noticed upon the introduction of the various inorganic salts, the effect was more pronounced in the presence of $CaCl_2$. Such a minor decrease in degradation efficiency could be attributed to the possible adsorption of Cl^- on the surface of FeZ-8 catalyst, thereby blocking some active sites [53] or because Cl^- might act as a hydroxyl radicals scavenger, as shown in Equation (4) below [54,55]:

$$Cl^- + {}^{\bullet}OH \rightarrow Cl^{\bullet} + OH^- \quad (4)$$

2.6.10. TOC Removal Studies

The catalytic activity of the FeZ-8 catalyst was further investigated by determining the total organic carbon (TOC) concentration of the OFL solution after the establishment of the adsorption–desorption equilibrium and Fenton degradation for 120 min, and the results are shown in Figure 8. Although the TOC removal efficiency was approximately 40% after the establishment of the adsorption–desorption equilibrium, the efficiency reached more than 50% after 120 min of Fenton degradation reaction. Such results confirmed that the FeZ-8 catalyst is capable of mineralizing the fluoroquinolone antibiotic.

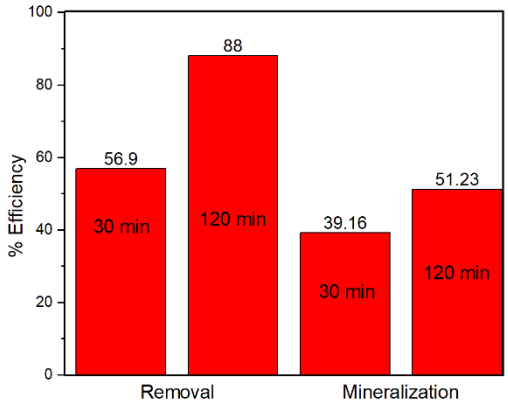

Figure 8. Total organic carbon (TOC) removal using FeZ-8.

2.6.11. Hetero-Fenton Degradation Mechanism

The reaction pathway for OFL degradation using the FeZ composite as a hetero-Fenton catalyst has been proposed and is schematically shown in Figure 9. The first stage involves the in-dark adsorption of OFL onto the surface of the FeZ composite catalyst. The Fe_3O_4 in FeZ is composed of Fe^{2+} and Fe^{3+}. The Fe^{2+} ions react with H_2O_2 to form HO• and more Fe^{3+} (Equation (5)). The HO• is responsible for

the degradation of OFL into CO_2, H_2O, and other intermediates. However, the H_2O_2 further reduces the Fe^{3+} back to Fe^{2+} (Equation (7)) and the cycle continues.

$$Fe^{2+} + H_2O_2 \rightarrow Fe^{3+} + OH^- + HO^{\bullet} \quad (5)$$

$$Fe^{3+} + H_2O_2 \rightarrow Fe^{2+} + H^+ + HO_2^{\bullet} \quad (6)$$

$$OFL + OH^{\bullet} \rightarrow CO_2 + H_2O + intermediates \quad (7)$$

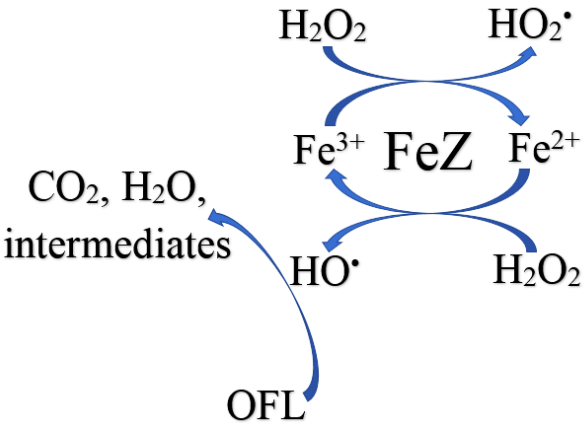

Figure 9. Proposed reaction pathway for OFL degradation using FeZ composite as hetero-Fenton catalyst.

2.6.12. Reusability and Stability Studies

A reusability study was conducted to investigate the stability of the FeZ-8 catalyst during repeated cycles. As shown in Figure 10a, the performance of the FeZ-8 catalyst after the fifth cycle remained significant, as the marginal drop in the efficiency is still below 10%, an indication that the FeZ-8 catalyst is reusable. The stability of the FeZ-8 catalyst was confirmed by examining the FTIR spectra of the catalyst before and after five cycles of repeated Fenton degradation studies, and no obvious difference exists between the two FTIR spectra of the FeZ-8 catalyst.

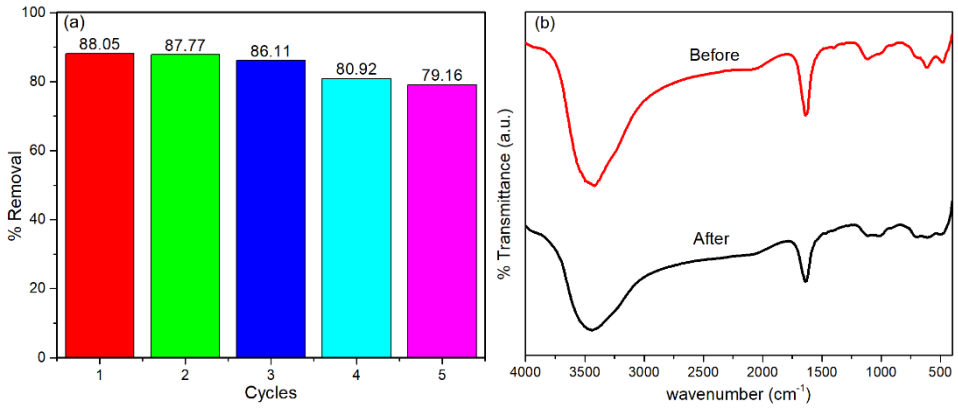

Figure 10. (**a**) Reusability studies of Fenton degradation of OFL using FeZ-8. (**b**) FTIR spectra of FeZ-8 catalyst before and after the Fenton degradation of OFL.

3. Materials and Methods

3.1. Chemicals

Ferric chloride hexahydrate ($FeCl_3{\cdot}6H_2O$), sodium chloride (NaCl), and calcium chloride ($CaCl_2$) were obtained from Bendosen (Shah Alam, Selangor, Malaysia). Hydrogen peroxide (H_2O_2), nitric acid (HNO_3), ethanol (CH_3CH_2OH), and sodium hydroxide (NaOH) were obtained from QReC Chemicals (Rawang; Selangor Malaysia). Sodium peroxydisulfate (PDS, $Na_2S_2O_8$), hydrochloric acid (HCl), and ammonia solution were obtained from Merck Chemicals (Darmstadt, Germany). Iron (II) sulfate heptahydrate ($FeSO_4{\cdot}7H_2O$) and zeolite were obtained from Sigma-Aldrich (Saint Louis, MO, USA). Potassium chloride (KCl) was obtained from Fluka (St. Gallen, Switzerland), while potassium peroxomonosulfate (PMS, $2KHSO_5{\cdot}KHSO_4{\cdot}K_2SO_4$) was supplied by Acros Organics (Morris, NJ, USA). All chemicals were of analytical grade and deionized water was used throughout.

3.2. Preparation of FeZ Composites

Fe_3O_4-zeolite (FeZ) composites were synthesized using the co-precipitation method [23]. Briefly, equimolar amounts (1.5, 3, 5, 8, or 10 mmol) of $FeSO_4{\cdot}7H_2O$ and FeCl3·6H2O were dissolved in 60 mL of 10 mmol L^{-1} aqueous HCl solution and heated to 80 °C (Solution A). Subsequently, 0.5 g of zeolite was introduced into solution A and stirred for 1 h (Solution B). Then, 40 mL of ammonia solution was added slowly into solution B and stirred together for 2 h, to form FeZ composites. Finally, the product was filtered, washed several times with distilled water and absolute ethanol, before being dried in an oven at 60 °C overnight. The composites were named FeZ-1.5, FeZ-3, FeZ-5, FeZ-8, and FeZ-10, based on the equimolar amount of iron precursors used during the synthesis.

3.3. Characterizations

The morphologies of the catalysts were determined using a transmission electron microscope (TEM) (model: Technai G2 F20, Eindhoven, Netherlands) and field emission scanning electron microscope (model: Leo Supra 50 VP FESEM, Eindhoven, Netherlands) accompanied with an energy dispersive X-ray detector (EDX) to determine the elemental composition of the catalysts. FTIR spectra were recorded with KBr pressed disks using a Perkin Elmer 2000 spectrometer (Beaconsfied, England). X-ray photoelectron spectroscopy (XPS) analysis was carried out using an ULVAC-PHI Quantera II XPS system with a monochromatic Al K-Alpha source (Chigasaki, Japan). The specific surface area of the catalysts was measured by the Brunauer–Emmett–Teller (BET) method using a Micromeritics ASAP (model 2020 V 4.01) surface area and porosity analyzer (Norcross, GA, USA).

3.4. Heterogeneous Fenton Degradation of OFL

The catalytic activity of FeZ composites was evaluated by degrading OFL in the presence of H_2O_2 in ambient conditions. In a typical procedure, 0.1 g of the catalyst was added into a 100 mL (20 ppm) aqueous OFL solution. The mixture was continuously stirred for 30 min in the dark in order to disperse FeZ catalyst and establish an adsorption–desorption equilibrium. Subsequently, 0.5 mL of aqueous H_2O_2 solution (30% *w*/*w*) was added to the mixture so as to enhance the catalytic performance via Fenton reaction. At a regular time interval, 5 mL of the reaction suspension was sampled and centrifuged immediately to separate the catalyst from the solution. The remnant OFL concentration in the supernatant was then determined at 286 nm using a Shimadzu UV 2600 spectrophotometer (version 1.03) operating using a UV probe 2.42. The effects of experimental conditions such as Fe_3O_4 loading on zeolite, catalyst loading, initial solution pH, initial OFL concentration, different oxidants, H_2O_2 dosage, reaction temperature, and inorganic salts were studied in order to determine the performance of FeZ catalyst towards the degradation of OFL under different conditions. The amount of Fe_3O_4 loaded on zeolite was varied from 1.5 to 10 mmol; catalyst dosage was varied from 0.25 to 2 $g{\cdot}L^{-1}$; initial solution pH was adjusted between 5 and 11 using HNO_3 or NaOH; initial OFL concentration was varied between 20 and 100 ppm; different oxidants such as potassium peroxomonosulfate, sodium

peroxydisulfate, and hydrogen peroxide; dosage of H_2O_2 from 1 to 20 mL·L^{-1}; reaction temperature between 25 and 60 °C; and different inorganic salts such as NaCl, KCl, and $CaCl_2$. The efficiency of the FeZ composite towards the removal (both adsorption and Fenton degradation) of OFL was calculated using Equation (8):

$$\% \, Removal = \frac{C_o - C_t}{C_o} \times 100\% \quad (8)$$

where C_o and C_t are the initial and the concentration of OFL solution at time t. Total organic carbon (TOC) was determined using a Shimadzu TOC-L analyzer. Finally, the reusability and stability of the catalyst were also studied.

4. Conclusions

Fe_3O_4-zeolite (FeZ) composites were synthesized via a facile co-precipitation method and were subsequently characterized using XPS, FTIR, FESEM-EDX, TEM, and BET, which successfully confirmed the immobilization of Fe_3O_4 onto zeolite. The immobilization of Fe_3O_4 onto zeolite resulted in the formation of FeZ composites with higher surface area and pore volume, compared to pristine zeolite. The effects of different operational parameters such as Fe_3O_4 loading on zeolite, catalyst loading, initial solution pH, initial OFL concentration, different oxidants, H_2O_2 dosage, reaction temperature, and inorganic salts on OFL degradation were systematically investigated. Among all the FeZ composites, the FeZ-8 composite exhibited a good catalytic capacity for the hetero-Fenton degradation of OFL. Under the reaction conditions of 1 g·L^{-1} catalyst dosage, pH of 9, and H_2O_2 dosage of 5mL·L^{-1}, 88% of OFL degradation efficiency and 51.3% of TOC removal efficiency were achieved using the FeZ-8 composite. Likewise, results from reusability tests revealed only a slight decrease in degradation ability after five runs. Therefore, the FeZ-8 composite could be a promising hetero-Fenton catalyst for the treatment of wastewater contaminated with antibiotics. A suitable hetero-Fenton degradation pathway has been proposed.

Supplementary Materials: The following are available online at http://www.mdpi.com/2073-4344/10/11/1241/s1, Figure S1: N2 adsorption-desorption isotherms and the corresponding pore size distribution (insets) for zeolite (a), FeZ-1.5 (b), FeZ-3 (c), FeZ-5 (d), FeZ-8 (e) and FeZ-10 (f) composites, Figure S2: (a) (C_0–C) versus t plots based on the zero-order kinetics model; (b) ln(C_0/C) versus t plots based on first-order kinetics model and (c) 1/C–1/C_0 versus t plots based on second order kinetics model for the effect of Fe_2O_3 loading on zeolite on the degradation of OFL, Table S1: Parameters of linear regression for different kinetic models in FeZ/H_2O_2 systems,

Author Contributions: Conceptualization, methodology, resources, and writing—review and editing, R.A.; writing—review and editing, W.D.O. and S.S.I.; investigation and writing—original draft preparation, A.R.D.A. All authors have read and agreed to the published version of the manuscript.

Funding: The authors gratefully acknowledged the financial support from Universiti Sains Malaysia under RUI Grant No. 1001/PKIMIA/8011117.

Conflicts of Interest: The authors declare no conflict of interest. The funders had no role in the design of the study; in the collection, analyses, or interpretation of data; in the writing of the manuscript, or in the decision to publish the results.

References

1. Wang, W.; Zhai, C.; Peng, Y.; Chao, K. A Nondestructive Detection Method for Mixed Veterinary Drugs in Pork Using Line-Scan Raman Chemical Imaging Technology. *Food Anal. Methods* **2019**, *12*, 658–667. [CrossRef]
2. Sharma, S.; Bhandari, A.; Choudhary, V.; Rajpurohit, H.; Khandelwal, P. RP-HPLC method for simultaneous estimation of nitazoxanide and ofloxacin in tablets. *Ind. J. Pharm. Sci.* **2011**, *73*, 84. [CrossRef]
3. Janos, F.; Robin, G.C. *Analogue-based Drug Discovery*, 1st ed.; Wiley-VCH: Hoboken, NJ, USA, 2006; ISBN 9783527607495.
4. Sun, J.; Song, M.; Feng, J.; Pi, Y. Highly efficient degradation of ofloxacin by UV/Oxone/Co^{2+} oxidation process. *Environ. Sci. Pollut. Res.* **2012**, *19*, 1536–1543. [CrossRef]

5. Chen, T.S.; Kuo, Y.M.; Chen, J.L.; Huang, K.L. Anodic degradation of ofloxacin on a boron-doped diamond electrode. *Int. J. Electrochem. Sci.* **2013**, *8*, 7625–7633.
6. Elfiky, M.; Salahuddin, N.; Hassanein, A.; Matsuda, A.; Hattori, T. Detection of antibiotic Ofloxacin drug in urine using electrochemical sensor based on synergistic effect of different morphological carbon materials. *Microchem. J.* **2019**, *146*, 170–177. [CrossRef]
7. Peres, M.; Maniero, M.; Guimarães, J. Photocatalytic degradation of ofloxacin and evaluation of the residual antimicrobial activity. *Photochem. Photobiol. Sci.* **2015**, *14*, 556–562. [CrossRef]
8. Enick, O.V.; Moore, M.M. Assessing the assessments: Pharmaceuticals in the environment. *Environ. Impact Assess. Rev.* **2007**, *27*, 707–729. [CrossRef]
9. Esposito, B.R.; Capobianco, M.L.; Martelli, A.; Navacchia, M.L.; Pretali, L.; Saracino, M.; Zanelli, A.; Emmi, S.S. Advanced water remediation from ofloxacin by ionizing radiation. *Radiat. Phys. Chem.* **2017**, *141*, 118–124. [CrossRef]
10. Wuana, R.A.; Sha'Ato, R.; Iorhen, S. Aqueous phase removal of ofloxacin using adsorbents from Moringa oleifera pod husks. *Adv. Environ. Res.* **2015**, *4*, 49–68. [CrossRef]
11. La Farre, M.; Pérez, S.; Kantiani, L.; Barceló, D. Fate and toxicity of emerging pollutants, their metabolites and transformation products in the aquatic environment. *TrAC Trends Anal. Chem.* **2008**, *27*, 991–1007. [CrossRef]
12. Dong, R.; Yu, G.; Guan, Y.; Wang, B.; Huang, J.; Deng, S.; Wang, Y. Occurrence and discharge of pharmaceuticals and personal care products in dewatered sludge from WWTPs in Beijing and Shenzhen. *Emerg. Contam.* **2016**, *2*, 1–6. [CrossRef]
13. Zhang, T. Antibiotics and resistance genes in wastewater treatment plants. *AMR Control* **2016**, *9*, 11–20.
14. Varjani, S.J.; Sudha, M.C. Treatment Technologies for Emerging Organic Contaminants Removal from Wastewater. In *Water Remediation*; Springer Nature: Singapore, 2018; pp. 91–115.
15. Cuerda-Correa, E.M.; Alexandre-Franco, M.F.; Fernández-González, C. Advanced oxidation processes for the removal of antibiotics from water. An overview. *Water* **2020**, *12*, 102. [CrossRef]
16. Jaafarzadeh, N.; Kakavandi, B.; Takdastan, A.; Kalantary, R.R.; Azizi, M.; Jorfi, S. Powder activated carbon/Fe_3O_4 hybrid composite as a highly efficient heterogeneous catalyst for Fenton oxidation of tetracycline: Degradation mechanism and kinetic. *RSC Adv.* **2015**, *5*, 84718–84728. [CrossRef]
17. Cleveland, V.; Bingham, J.P.; Kan, E. Heterogeneous Fenton degradation of bisphenol A by carbon nanotube-supported Fe_3O_4. *Sep. Purif. Technol.* **2014**, *133*, 388–395. [CrossRef]
18. Hua, Z.; Ma, W.; Bai, X.; Feng, R.; Yu, L.; Zhang, X.; Dai, Z. Heterogeneous Fenton degradation of bisphenol A catalyzed by efficient adsorptive Fe_3O_4/GO nanocomposites. *Environ. Sci. Pollut. Res.* **2014**, *21*, 7737–7745. [CrossRef]
19. Mazilu, I.; Ciotonea, C.; Chirieac, A.; Dragoi, B.; Catrinescu, C.; Ungureanu, A.; Petit, S.; Royer, S.; Dumitriu, E. Synthesis of highly dispersed iron species within mesoporous (Al-) SBA-15 silica as efficient heterogeneous Fenton-type catalysts. *Microporous Mesoporous Mater.* **2017**, *241*, 326–337. [CrossRef]
20. Krishna, L.S.; Soontarapa, K.; Asmel, N.K.; Kabir, M.A.; Yuzir, A.; Yaacob, W.Z.W.; Sarala, Y. Adsorption of acid blue 25 from aqueous solution using zeolite and surfactant modified zeolite. *Desalin. Water Treat.* **2019**, *150*, 348–360. [CrossRef]
21. De Sousa, D.N.R.; Insa, S.; Mozeto, A.A.; Petrovic, M.; Chaves, T.F.; Fadini, P.S. Equilibrium and kinetic studies of the adsorption of antibiotics from aqueous solutions onto powdered zeolites. *Chemosphere* **2018**, *205*, 137–146. [CrossRef]
22. Zhu, D.; Liu, S.; Chen, M.; Zhang, J.; Wang, X. Flower-like-flake Fe_3O_4/g-C_3N_4 nanocomposite: Facile synthesis, characterization, and enhanced photocatalytic performance. *Colloids Surf. A Physicochem. Eng. Asp.* **2018**, *537*, 372–382. [CrossRef]
23. Huang, R.; Fang, Z.; Yan, X.; Cheng, W. Heterogeneous sono-Fenton catalytic degradation of bisphenol A by Fe_3O_4 magnetic nanoparticles under neutral condition. *Chem. Eng. J.* **2012**, *197*, 242–249. [CrossRef]
24. Adimoolam, M.G.; Amreddy, N.; Nalam, M.R.; Sunkara, M.V. A simple approach to design chitosan functionalized Fe_3O_4 nanoparticles for pH responsive delivery of doxorubicin for cancer therapy. *J. Magn. Magn. Mater.* **2018**, *448*, 199–207. [CrossRef]
25. Caglar, B.; Guner, E.K.; Keles, K.; Özdokur, K.V.; Cubuk, O.; Coldur, F.; Caglar, S.; Topcu, C.; Tabak, A. Fe_3O_4 nanoparticles decorated smectite nanocomposite: Characterization, photocatalytic and electrocatalytic activities. *Solid State Sci.* **2018**, *83*, 122–136. [CrossRef]

26. Zhao, H.; Weng, L.; Cui, W.W.; Zhang, X.R.; Xu, H.Y.; Liu, L.Z. In situ anchor of magnetic Fe_3O_4 nanoparticles onto natural maifanite as efficient heterogeneous Fenton-like catalyst. *Front. Mat. Sci.* **2016**, *10*, 300–309. [CrossRef]
27. Karami, B.; Hoseini, S.J.; Eskandari, K.; Ghasemi, A.; Nasrabadi, H. Synthesis of xanthene derivatives by employing Fe_3O_4 nanoparticles as an effective and magnetically recoverable catalyst in water. *Catal. Sci. Technol.* **2012**, *2*, 331–338. [CrossRef]
28. Zhao, T.; Ji, X.; Guo, X.; Jin, W.; Dang, A.; Li, H.; Li, T. Preparation and electrochemical property of Fe_3O_4/MWCNT nanocomposite. *Chem. Phy. Lett.* **2016**, *653*, 202–206. [CrossRef]
29. Liu, Y.; Xu, J.; Wang, L.; Zhang, H.; Xu, P.; Duan, X.; Sun, H.; Wang, S. Three-dimensional BiOI/BiOX (X = Cl or Br) nanohybrids for enhanced visible-light photocatalytic activity. *Nanomaterials* **2017**, *7*, 64. [CrossRef]
30. Liao, Q.; Sun, J.; Gao, L. Degradation of phenol by heterogeneous Fenton reaction using multi-walled carbon nanotube supported Fe_2O_3 catalysts. *Colloids Surf. A Physicochem. Eng. Asp.* **2009**, *345*, 95–100. [CrossRef]
31. Hassan, H.; Hameed, B. Fe–clay as effective heterogeneous Fenton catalyst for the decolorization of Reactive Blue 4. *Chem. Eng. J.* **2011**, *171*, 912–918. [CrossRef]
32. Hu, X.; Liu, B.; Deng, Y.; Chen, H.; Luo, S.; Sun, C.; Yang, P.; Yang, S. Adsorption and heterogeneous Fenton degradation of 17α-methyltestosterone on nano Fe_3O_4/MWCNTs in aqueous solution. *Appl. Catal. B Environ.* **2011**, *107*, 274–283. [CrossRef]
33. Lan, H.; Wang, A.; Liu, R.; Liu, H.; Qu, J. Heterogeneous photo-Fenton degradation of acid red B over Fe_2O_3 supported on activated carbon fiber. *J. Hazard. Mat.* **2015**, *285*, 167–172. [CrossRef]
34. Tian, Y.; He, X.; Zhou, H.; Tian, X.; Nie, Y.; Zhou, Z.; Yang, C.; Li, Y. Efficient fenton-like degradation of ofloxacin over bimetallic Fe–Cu@ Sepiolite composite. *Chemosphere* **2020**, *257*, 127209. [CrossRef]
35. Wang, X.; Jin, H.; Wu, D.; Nie, Y.; Tian, X.; Yang, C.; Zhou, Z.; Li, Y. Fe_3O_4@S-doped ZnO: A magnetic, recoverable, and reusable Fenton-like catalyst for efficient degradation of ofloxacin under alkaline conditions. *Environ. Res.* **2020**, *186*, 109626. [CrossRef]
36. Liu, J.; Wu, X.; Liu, J.; Zhang, C.; Hu, Q.; Hou, X. Ofloxacin degradation by Fe_3O_4-CeO_2/AC Fenton-like system: Optimization, kinetics, and degradation pathways. *Mole. Cat.* **2019**, *465*, 61–67. [CrossRef]
37. Zheng, C.; Yang, C.; Cheng, X.; Xu, S.; Fan, Z.; Wang, G.; Wang, S.; Guan, X.; Sun, X. Specifically enhancement of heterogeneous Fenton-like degradation activities for ofloxacin with synergetic effects of bimetallic Fe-Cu on ordered mesoporous silicon. *Sep. Purif. Technol.* **2017**, *189*, 357–365. [CrossRef]
38. Azizan, Z.; Azran, M.; Hassan, H.; Faraziehan, S.; Abu Hassan, N. Decolorization of Reactive Black 5 using Fe-areca nut as a heterogeneous Fenton catalyst. *Proc. Appl. Mech. Mater.* **2014**, *661*, 29–33. [CrossRef]
39. Soon, A.N.; Hameed, B. Degradation of Acid Blue 29 in visible light radiation using iron modified mesoporous silica as heterogeneous Photo-Fenton catalyst. *Appl. Catal. A Gen.* **2013**, *450*, 96–105. [CrossRef]
40. Shukla, P.; Wang, S.; Sun, H.; Ang, H.-M.; Tadé, M. Adsorption and heterogeneous advanced oxidation of phenolic contaminants using Fe loaded mesoporous SBA-15 and H_2O_2. *Chem. Eng. J.* **2010**, *164*, 255–260. [CrossRef]
41. Nguyen, T.D.; Phan, N.H.; Do, M.H.; Ngo, K.T. Magnetic Fe_2MO_4 (M: Fe, Mn) activated carbons: Fabrication, characterization and heterogeneous Fenton oxidation of methyl orange. *J. Hazard. Mat.* **2011**, *185*, 653–661. [CrossRef] [PubMed]
42. Yu, L.; Chen, J.; Liang, Z.; Xu, W.; Chen, L.; Ye, D. Degradation of phenol using Fe_3O_4-GO nanocomposite as a heterogeneous photo-Fenton catalyst. *Sep. Purif. Technol.* **2016**, *171*, 80–87. [CrossRef]
43. Li, W.; Wan, D.; Wang, G.; Chen, K.; Hu, Q.; Lu, L. Heterogeneous Fenton degradation of Orange II by immobilization of Fe_3O_4 nanoparticles onto Al-Fe pillared bentonite. *Korean J. Chem. Eng.* **2016**, *33*, 1557–1564. [CrossRef]
44. Tang, X.; Feng, Q.; Liu, K.; Li, Z.; Wang, H. Fabrication of magnetic Fe_3O_4/silica nanofiber composites with enhanced Fenton-like catalytic performance for Rhodamine B degradation. *J. Mat. Sci.* **2018**, *53*, 369–384. [CrossRef]
45. Shi, X.; Tian, A.; You, J.; Yang, H.; Wang, Y.; Xue, X. Degradation of organic dyes by a new heterogeneous Fenton reagent-Fe_2GeS_4 nanoparticle. *J. Hazard. Mat.* **2018**, *353*, 182–189. [CrossRef] [PubMed]
46. Wang, Y.; Lu, J.; Wu, J.; Liu, Q.; Zhang, H.; Jin, S. Adsorptive removal of fluoroquinolone antibiotics using bamboo biochar. *Sustainability* **2015**, *7*, 12947–12957. [CrossRef]

47. Khan, J.A.; He, X.; Khan, H.M.; Shah, N.S.; Dionysiou, D.D. Oxidative degradation of atrazine in aqueous solution by UV/H_2O_2/Fe^{2+}, UV/$S_2O_8^{2-}$/Fe^{2+} and UV/HSO_5^-/Fe^{2+} processes: A comparative study. *Chem. Eng. J.* **2013**, *218*, 376–383. [CrossRef]
48. Du, J.; Wang, Y.; Xu, T.; Zheng, H.; Bao, J. Synergistic degradation of PNP via coupling H_2O_2 with persulfate catalyzed by nano zero valent iron. *RSC Adv.* **2019**, *9*, 20323–20331. [CrossRef]
49. Ji, Y.; Wang, L.; Jiang, M.; Yang, Y.; Yang, P.; Lu, J.; Ferronato, C.; Chovelon, J.M. Ferrous-activated peroxymonosulfate oxidation of antimicrobial agent sulfaquinoxaline and structurally related compounds in aqueous solution: Kinetics, products, and transformation pathways. *Environ. Sci. Pollut. Res.* **2017**, *24*, 19535–19545. [CrossRef]
50. Liu, Y.; Jin, W.; Zhao, Y.; Zhang, G.; Zhang, W. Enhanced catalytic degradation of methylene blue by α-Fe_2O_3/graphene oxide via heterogeneous photo-Fenton reactions. *Appl. Catal. B Environ.* **2017**, *206*, 642–652. [CrossRef]
51. Feng, J.; Hu, X.; Yue, P.L. Novel bentonite clay-based Fe- nanocomposite as a heterogeneous catalyst for photo-fenton discoloration and mineralization of orange II. *Environ. Sci. Technol.* **2004**, *38*, 269–275. [CrossRef]
52. Chen, F.; Xie, S.; Huang, X.; Qiu, X. Ionothermal synthesis of Fe_3O_4 magnetic nanoparticles as efficient heterogeneous Fenton-like catalysts for degradation of organic pollutants with H_2O_2. *J. Hazard. Mat.* **2017**, *322*, 152–162. [CrossRef]
53. Wen, X.J.; Niu, C.G.; Zhang, L.; Liang, C.; Zeng, G.M. An in depth mechanism insight of the degradation of multiple refractory pollutants via a novel $SrTiO_3$/BiOI heterojunction photocatalysts. *J. Catal.* **2017**, *356*, 283–299. [CrossRef]
54. Tsuneda, S.; Ishihara, Y.; Hamachi, M.; Hirata, A. Inhibition effect of chlorine ion on hydroxyl radical generation in UV-H_2O_2 process. *Water Sci. Technol.* **2002**, *46*, 33–38. [CrossRef]
55. Dugandžić, A.M.; Tomašević, A.V.; Radišić, M.M.; Šekuljica, N.Ž.; Mijin, D.Ž.; Petrović, S.D. Effect of inorganic ions, photosensitisers and scavengers on the photocatalytic degradation of nicosulfuron. *J. Photochem. Photobiol. A Chem.* **2017**, *336*, 146–155. [CrossRef]